Periodic Forcing of Inhibition-Stabilized Networks: Nonlinear Resonances and Phase-Amplitude Coupling

Romain Veltz, Terrence J. Sejnowski

Periodic forcing of stabilized E-I networks: Nonlinear resonance curves and dynamics

Romain Veltz[1, 2]

[1]Howard Hughes Medical Institute, Salk Institute for Biological Studies, La Jolla, CA 92037, USA

[2]INRIA Sophia Antipolis Mediterrane, France

Terrence J. Sejnowski[1, 2]

[1]Howard Hughes Medical Institute, Salk Institute for Biological Studies, La Jolla, CA 92037, USA

[2]Division of Biological Sciences, University of California San Diego, La Jolla, CA 92093 USA

Keywords: Oscillation, gamma band, theta band

Abstract

Inhibition stabilized networks (ISNs) are neural architectures with strong positive feedback among pyramidal neurons balanced by strong negative feedback from inhibitory interneurons, a circuit element found in the hippocampus and the primary visual cortex. In their working regime, ISNs produce damped oscillations in the γ-range in response to inputs to the inhibitory population. In order to understand the properties of interconnected ISNs, we investigated periodic forcing of ISNs. We show that ISNs can be excited over a range of frequencies and derive properties of the resonance peaks. In particular, we studied the phase-locked solutions, the torus solutions and the resonance peaks. More particular, periodically forced ISNs respond with (possibly multi-stable) phase-locked activity whereas networks with sustained intrinsic oscillations respond more dynamically to periodic inputs with tori. Hence, the dynamics are surprisingly rich and phase effects alone do not adequately describe the network response. This strengthens the importance of phase-amplitude coupling as opposed to phase-phase coupling in providing multiple frequencies for multiplexing and routing information.

1 Introduction

Oscillatory rhythms of neuronal populations are ubiquitous in the brain (see (Buzsaki 2004) for a review) but their functions are not yet established (Sejnowski 2006). Gamma oscillations in the 30-80 Hz frequency band (Bartos 2007) have been implicated in attention and memory, in coding information, in communication between brain areas

(Buzski 1995; Bichot 2005; Ray 2011; Womelsdorf 2012; Igarashi 2014) and are abnormal in pathologies such as schizophrenia (Lewis 2005), autism (Wright 2012) and Parkinson's disease (Hemptinne 2013).

Gamma frequency oscillations are often coupled with oscillations at lower frequencies (Jensen 2007). For example, oscillating inputs to the hippocampus from the medial septum are in the theta frequency range (4-8 Hz). CA1 neurons in hippocampus also receive inputs from the medial entorhinal cortex in the high gamma frequency range (60-80) Hz, and inputs from the CA3 neuron in the low gamma frequency range (30-60 Hz) (Colgin 2009). When neural networks in these different regions are coupled, there is an interplay between oscillations that are internally generated and those that arise from external inputs.

Analyzing these networks theoretically is difficult (Borisyuk 1995), even at the scale of neural populations because the interplay of multiple frequencies may lead to chaotic behavior (Newhouse 1978). Large-scale network models of these oscillations also have large numbers of parameters, which are difficult to analyze (Vierling-Claassen 2008). However this analysis can be more easily undertaken in models with fewer parameters and the intrinsic working regimes of the different neural populations are known. A good example of this is (Tsodyks 1997), which analyzed a neural model of hippocampal circuits forced by inputs from the medial septum (see Figure 1). This network consisted of two populations of interconnected neurons, excitatory and inhibitory, such that when the inhibitory connections are removed, the remaining excitatory network is unstable. Network stability was maintained by strong inhibitory connections, putting the network into a dynamical regime called an Inhibition Stabilized Network (ISN). Recently, ISNs

have been used to model cortical visual area (Murphy 2009; Ozeki 2009; Jadi 2014a; Jadi 2014b) and they can also be found in studies where the ISN regime is not explicitly invoked (Kang 2010; Akam 2012).

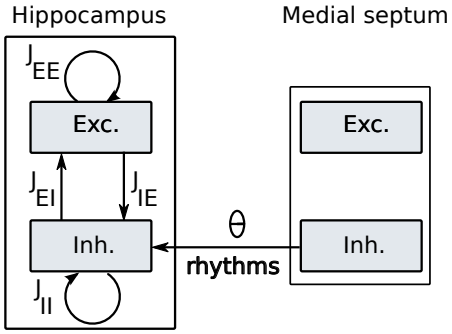

Figure 1: Entrainment of theta activity in hippocampus by rhythmic inhibition of inhibitory interneurons.

Two properties of these ISNs make them especially interesting. First, increasing the direct external inhibitory input to the inhibitory interneurons causes the interneurons paradoxically to decrease their firing rates, and, second, the ISN operating regime supports intrinsic gamma oscillations.

The main objective of the present study is to understand the amplification of gamma rhythms of networks driven by periodic external inputs when the gamma rhythm are generated resonantly within the circuitry of the network.

To this end, we focus on the ISN which, as we will see, can be understood as damped oscillators. There are several reasons to perform this analysis in addition to the above considerations:

1. An extension of (Tsodyks 1997) is to assume that the hippocampus contains interconnected ISNs. As a first step toward the study of such networks, we can consider a feedforward chain of two ISNs and the even simpler case where the last ISN of the chain is periodically forced (by the first ISN)

2. ISNs have been shown to be relevant for the description of the local circuitry of V1 (see the experimental paper (Ozeki 2009)): interconnected ISNs would then be adequate for the study of center/surround interactions,

3. It has been shown recently (Akam 2012) that a firing rate model of CA3 neuron with sustained oscillations can be used to fit the phase response curve (PRC) of carbachol induced oscillations as well as optogenetic stimulation. The PRC is a tool (Ermentrout 2010) valid far from a bifurcation point. This suggests that the PRC is inadequate for the study of forced ISNs where phase-amplitude coupling may arise (Aronson 1990).

Periodic forcing of neural oscillators is a well studied paradigm but most papers are not applicable to periodic forcing of ISN because they assume, first, that the oscillations are sustained (see for example (Neu 1979; Ermentrout 1981)); second, that the forcing amplitude is small compared to the amplitude of the network oscillations; and the third concerns the forcing frequency ω_F, which is off resonance with an intrinsic frequency ω_H *i.e.* that is not related by a rational number; as a consequence, resonance effects are ignored (see for example (Hoppensteadt 1997)).

One notable exception to the first assumption is (Aronson 1990), although resonance conditions were not addressed. These above assumptions naturally lead to the

limited description of phase-locked (PL) solutions, that are ω_F-periodic solutions with constant amplitude. Hence, the only variable in these solutions is the relative phase between the forcing and the output which is assumed to encode information. This scheme is called phase-phase coupling in the literature.

Here, we go beyond a phase description and look at how the amplitude of the response is affected by nonlinear resonance effects. The resonance effect in which a network with intrinsic frequency ω_H displays a maximum in the amplitude of the response when the forcing frequency ω_F is close to ω_H, has been known for some time. It was used recently in experiments (Cardin 2009) to investigate the neural mechanism responsible for gamma oscillations in the barrel cortex. It has been used in (Akam 2010) to show how to multiplex information and also in (Paik 2010) to show how the visual cortex can adjust its working regime to the frequency content of the thalamus inputs.

When the system is nonlinear, theory predicts that resonances appear at every rational ratio k/l of ω_F/ω_H although in real oscillatory systems, the maximum and width of the resonance decrease with $|k| + |l|$: resonances only occur for frequency ratios $1/2, 1$ and 2. The detuning parameter $\delta\omega \stackrel{def}{=} \omega_H - \frac{k}{l}\omega_F$ is a fundamental parameter for the description of the $k : l$ resonance peak. Compared to linear resonance, many more new network responses can be produced. For sub-harmonic forcing $\omega_F < \omega_H$, the PL frequency is the same as the forcing frequency. For super-harmonic forcing $\omega_H < \omega_F$, the periodic responses frequencies are a fraction of the forcing frequency $\frac{\omega_F}{l}$ thereby producing again a phase-locked (to the input) solution. Hence, we will also call them PL. In addition, there can be multi-stability of PL and also modulated responses with two intrinsic frequencies that we call *torus* solutions or quasiperiodic solutions. The *reso-*

nance curve is then the amplitude of the response (PL/torus) as function of the forcing frequency ω_F.

In earlier work along these lines (Pollina 2003; Ledoux 2011; Decker 2012) the multi-stability of PL solutions was studied around the $1:1$ peak. One can find a resonance curve in the periodic forcing of spatially extended ISN networks in (Rule 2011). Resonance effects in neural masses have also been studied in (Spiegler 2011), though without addressing dynamics. There are general limitations to the phase description of neural oscillators (PRC), namely the allowed size for the perturbation can be small. (Wedgwood 2013) gives the example of Morris-Lecar neurons forced by periodic kicks, producing chaotic response, and provides an adequate phase-amplitude description.

Understanding the properties of the resonances of an oscillatory system is extremely difficult in general. Here, by looking at the ISN, which we show are tuned close to a Hopf bifurcation, we are able to understand thoroughly the possible network responses PL/torus. The periodic forcing of a Hopf bifurcation has been studied in (Gambaudo, J. M. 1985) where all the responses were listed near all resonances. However, the link with our model is buried in multiple changes of variables. Recently, the resonance curves were classified in (Zhang 2011) around the $1:1$ resonance. The first issue with this study is that the description of the torus solutions is lacking, hence the resonances curves are incomplete as the authors focused solely on PL solutions. The second issue is that they do not provide the stability of the PL responses limiting the predicxtive power of the analysis. In this work, we compute the changes of variables that provide the normal form as in (Gambaudo, J. M. 1985) and we also provide several formulas concerning the resonance curves. This is technical, lengthy but not too diffi-

cult (see appendices). This allows us to understand the resonance curves completely. In passing, we re-discover some results exposed in (Zhang 2011).

Finally, we introduce a type of network similar to the ISN but which supports sustained oscillations (SO), for example those that are induced by carbachol. The E/I network that we then consider can be tuned to either the ISN or the SO regime.

The plan of the study is as follows. After presenting the model and the general method - which is mainly the use of bifurcation theory - we tune an unforced E-I network to support the ISN behaviors. Then, we study in detail the main resonances $1:1, 1:2, 2:1$. A discussion follows.

2 Description of the model and definitions

In this work, we analyze a rate model with two populations of excitatory and inhibitory neurons (E/I network). More specifically, we consider a Wilson and Cowan model describing the firing rate of each population:

$$\begin{cases} \tau_E \dot{E} &= -E + S(J_{EE}E + J_{EI}I + \theta_E(t)) \\ \tau_I \dot{I} &= -I + S(J_{IE}E + J_{II}I + \theta_I(t)) \end{cases} \tag{1}$$

where S is the sigmoid function

$$S(x) = \frac{1}{1+e^{-x}}.$$

The variables θ_E, θ_I describe the total presynaptic current onto each population and τ_E, τ_I are the time constants of each population. Finally, the connections are such that $J_{EE}, J_{IE} > 0$ and $J_{EI}, J_{II} < 0$. The total presynaptic currents $(\theta_E(t), \theta_I(t))$ are sup-

posed to be periodic functions of time with only one Fourier component:

$$\begin{bmatrix} \theta_E(t) \\ \theta_I(t) \end{bmatrix} = \begin{bmatrix} \theta_E^{(0)} \\ \theta_I^{(0)} \end{bmatrix} + \epsilon \cos(\omega_F t) \begin{bmatrix} \theta_E^{(1)} \\ \theta_I^{(1)} \end{bmatrix} \tag{2}$$

where $\epsilon << 1$ is the (small) amplitude of the forcing and ω_F is the forcing frequency. An important quantity is the detuning. Consider a rational approximation of the ratio $\frac{\omega_H}{\omega_F} \approx \frac{k}{l}$ where ω_H is the gamma frequency of the rhythms generated by the E/I network, the detuning is defined by

$$\delta\omega \stackrel{def}{=} \omega_H - \frac{k}{l}\omega_F.$$

We call phase-locked (PL) solution a time-periodic network response of (1) with frequency ω_F/l, $l > 0$ integer, fraction of the forcing frequency. We call a quasiperiodic network response $V(t)$, or *torus* solution, a response with two frequency components $V(t) = f(\omega_1 t, \omega_2 t)$ where f 2π-periodic in each variable (see for example Figure 8 Top).

3 Methods

The reader versed to dynamical systems and bifurcation theory can skip this part. The goal of the present study is to understand the possible behaviors of the network (1) when the forcing frequency ω_F and the forcing amplitude ϵ are varied. To explain the method, it is best to re-write the equations as $\dot{V} = F(V, t, \mu)$ where $V = (E, I)$ and μ is the set of parameters. When $\epsilon = 0$, the system is autonomous and we write $F(V, t, \mu) \stackrel{\epsilon=0}{=} F^0(V, \mu)$. We first set the parameters μ such that the unforced network $\dot{V} = F^0(V, \mu)$ behaves like an ISN. Then we study the effects of the forcing terms. In particular, we

are interested in time-periodic and quasiperiodic solutions of (1), especially in their amplitude.

We recall that an *equilibrium* is a point V^f where the vector field $F^0(\cdot, \mu)$ vanishes. When the parameters μ are varied, any change of qualitative behavior will be called a *bifurcation*[1]. Often it corresponds to a change of stability or the creation of a behavior. These bifurcations can be detected by looking at the stability of the equilibrium which is stable if the eigenvalues of the Jacobian of F^0 at (V^f, μ) have negative real parts. When μ is varied, the eigenvalues of the equilibrium move smoothly in the complex plane: when two complex conjugate eigenvalues cross the imaginary axis for $\mu = \mu_H$ the system undergoes what is called a *Hopf* bifurcation signaling the appearance/disappearance of periodic solutions. The set of bifurcations points partitions the parameter space in sets of similar dynamics, this is called the *bifurcation diagram*. Close to a bifurcation point, the vector field F^0 can be simplified by a change of variables into its *normal form* that is the polynomial approximation with the least amount of monomials.

The study of the forced system is done as follows. Suppose that we can write the activity $V = V^f + z(t)e^{i\omega_H t}\zeta + c.c.$ where c.c. means complex conjugate and ζ is a 2d vector. We put this expression into the equations $\dot{V} = F(V, t, \mu)$ to derive a normal form for z like $\dot{z} = \alpha z + \beta z|z|^2 + \cdots$ which does not depend on time. Note that, when $z = 0$, the network response is an equilibrium whereas when $z(t) = z_0$, the network response is time periodic. Finally, a time periodic solution $z(t)$ corresponds to a torus network response. We can thus analyze the differential equation in z with bifurcation

[1] For more precise definitions, see (Guckenheimer 1983; Kuznetsov 1998).

theory to predict the different network responses and resonances.

3.1 ISN are tuned close to a supercritical Hopf bifurcation

We tune the parameters in order to select the adequate working regime for the ISN *i.e.* the parameter set that produces damped oscillations in the gamma range. An ISN satisfies the following properties (Tsodyks 1997):

1. when the inter-population connections $J_{IE} = J_{EI} = 0$ are zero, an equilibrium and more precisely the (stationary) excitatory firing rate E^f solution of $E^f = S(J_{EE}E^f + \theta_E)$, is unstable *i.e.* $-1 + J_{EE}S'(J_{EE}E^f + \theta_E) > 0$.

2. when the inter-populations connections are re-established, there is a stable equilibrium (E^f, I^f) solution of $(\dot{E} = \dot{I} = 0)$, is stable, which is when all the eigenvalues the Jacobian at (E^f, I^f) have negative real parts.

If we assume that it is the same equilibrium, at some point between these two extremes, the eigenvalues $\pm i\omega_H$ of the Jacobian at the equilibrium have zero real parts with nonzero imaginary parts: in general the network undergoes what is called a Hopf bifurcation signaling the appearance/disappearance of $\frac{2\pi}{\omega_H}$-periodic solutions. (see (Kuznetsov 1998)). Note that from point 1., an ISN requires J_{EE} to be relatively small.

We now freeze the connectivity and vary the total presynaptic currents to find the Hopf bifurcations where the network is tuned. The bifurcation diagram of eq (1) is well known (see for example (Wilson 1972; Borisyuk 1992; Hoppensteadt 1997)). The Hopf bifurcation curves (red) in the plane $(\theta_E^{(0)}, \theta_I^{(0)})$ are plotted in Figure 2 Left. The red shaded region corresponds to the parameters where the E/I network produces sustained

oscillations (SO). The gray shaded region in Figure 2 correspond to the ISN working regime with damped oscillations.

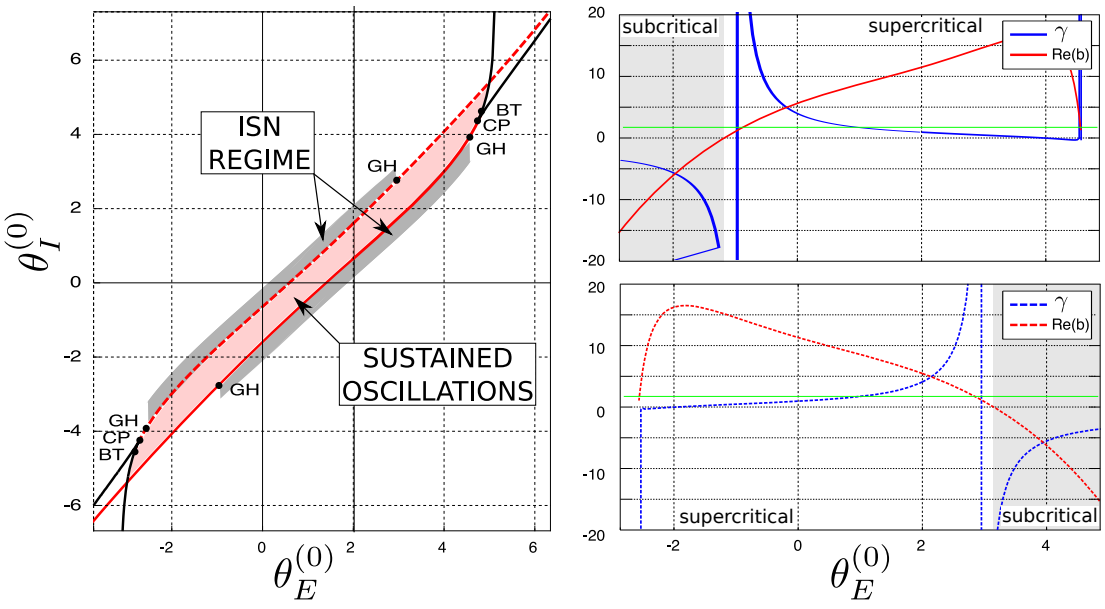

Figure 2: **Bifurcation diagram of the E/I network.** Left: Hopf bifurcation curves (red) and Fold bifurcation curves (black) in the plane $(\theta_E^{(0)}, \theta_I^{(0)})$, Generalized Hopf bifurcation point (GH), Bogdanov-Takens bifurcation point (BT), Cusp bifurcation point (CP). Right: Hopf normal form coefficient $\Re(b)$ (red) and shear γ (blue). The green curve equation is $y = \sqrt{3}$. Dashed and continuous curves correspond to the dashed and continuous Hopf curve, respectively, in the left panel. The ISN regions have a gray background. Parameters: $J_{EE} = 10$, $J_{EI} = -12$, $J_{IE} = 10$, $J_{II} = -10$ and $\tau_E/\tau_I = 3/8$. (Diagrams computed with the MatCont.)

Close to the Hopf curves (red), there is a good polynomial approximation of eq (1), called the Hopf normal form, whose coefficients are important in determining how the E/I network responds to constant inputs $\theta_E^{(0)}, \theta_I^{(0)}$. We will consider the case of the inhibitory current $\theta_I^{(0)}$ as a parameter. More precisely, if we call ζ the eigenvector of the

Jacobian for the eigenvalue $\imath\omega_H$ and we write

$$(E, I) = (E^f, I^f) + z\zeta + \bar{z}\bar{\zeta} + \Psi(z, \bar{z}) \tag{3}$$

where Ψ is a polynomials of order at least 2, hence negligible, then:

$$\dot{z} = z(\imath\omega_H + a\delta\theta_I^{(0)} - b|z|^2) + h.o.t. \tag{4}$$

where $\delta\theta_I^{(0)} \stackrel{def}{=} \theta_I^{(0)} - \theta_{I,Hopf}^{(0)}$ and $h.o.t.$ means polynomial terms in z hence negligible. To completely characterize the behavior of the network, we need to compute the complex coefficients a, b as function of the network parameters. Recall that the Hopf bifurcation is said *supercritical* (resp. *subcritical*) when $\Re b > 0$ (resp. $\Re b < 0$). Computing the *Lyapunov coefficient* b and the linear coefficient a is a daunting task even if an analytical expression exists (see for example (Guckenheimer 1983; Kuznetsov 1998)). Hence, we compute them here numerically. In figure 2 Right, we plot for each Hopf curve (dashed and continuous), the real part of b and the *shear* γ defined by

$$\gamma \stackrel{def}{=} \frac{\Im(b)}{\Re(b)}. \tag{5}$$

Writing eq (4) in polar coordinates, we see that the shear acts on the phase variable, speeding-up or slowing down the phase as function of the radius. Hence, it describes how the flow is distorted along the phase variable.

For the network response to an inhibitory transient input to produce damped oscillations (Tsodyks 1997), the working regime of the ISN should be close to a supercritical Hopf bifurcation. In contrast, close to a subcritical Hopf bifurcation with a bounded nonlinearity $S(x)$, the bifurcation diagram of eq (1) resembles that of a class II neuron, which exhibits an undesirable bistability between large amplitude oscillations and the

constant solution. Indeed, this may collide with the requirement of damped oscillations in response to a transient inhibitory input.

Definition 3.1. *We therefore assume that the ISN regime of a two-population network is close to a supercritical Hopf bifurcation where* $\Re b > 0$.

Let us look at the consequences of $\Re b > 0$, what follows is easily seen in polar coordinates for z. In the case, $\Re a\delta\theta_I^{(0)} > 0$, the stable response is given by $z(t) = \sqrt{\frac{\Re(a\delta\theta_I^{(0)})}{\Re b}}e^{i\omega_H t+\phi}$ which are network sustained oscillations. In the other case, the stable response is $z(t) = 0$. Thus, the term $\Re(a)\delta\theta_I^{(0)}$ controls which regime the network is in as summed up in table 3.1.

Regime	**Condition**
ISN	$\Re(a)\delta\theta_I^{(0)} < 0$
SO	$\Re(a)\delta\theta_I^{(0)} > 0$

Table 1: Link between the E/I network working regime with the internal parameters.

Rephrasing these mathematical results, we found that for a E-I network to work like an ISN, it requires to be tuned close to a Hopf bifurcation effectively acting as a Stuart-Landan oscillator which is described by eq (4), also called the normal form. The parameter $\Re(a)\delta\theta_I^{(0)}$ controls the network working regime, namely ISN *vs.* SO.

3.2 Numerical study of the phase-locked responses

With the network tuned as in the previous section, we study the effect of periodic presynaptic currents with forcing frequency ω_F (see eq (1)).

Definition 3.2. *A $k : l$ resonance occurs when the forcing frequency ω_F is a rational fraction of ω_H: $\frac{\omega_F}{\omega_H} = \frac{l}{k}$.*

For a given forcing amplitude, we compute numerically (software Auto07p) the PL responses as function of the forcing frequency as shown in Figure 3. The stable responses are shown in black and the unstable in dashed gray.

As is well known from linear theory, periodic forcing close to the intrinsic frequency ω_H leads to a large increase in the amplitude of the response characterized by a bell shape curve in the amplitude of the response *v.s.* forcing frequency called "resonance curve". This is seen in Figure 3 for $\omega_F \approx \omega_H$.

Because of the ISN being poised close to a Hopf bifurcation, several new phenomena arise. There seem to be additional peaks at ratios $3 : 1, 2 : 1$ and $1 : 2$. There is also multistability (Figure 3 Right) which was reported in (Decker 2012; Pollina 2003).

Note that the analysis of the PL solutions fails to predict the network response for $\omega_F \approx 1.5\omega_H$ in Figure 3 Right because the PL solutions are unstable. At this stage, we can already guess that the stable network response is a torus solution.

There is an important phenomenon near $\omega_F \approx 2\omega_H$ that we will explain more precisely in the following sections. When forced at frequency $2\omega_H$, the stable response of the network is a PL solution with frequency ω_H, *i.e.* there is a period doubling in the response of the network.

3.3 Theoretical properties of the network resonances

In this section, we study the nonlinear resonance curves using the normal form approximation. There are only a few systematic studies of periodic forcing of a Hopf

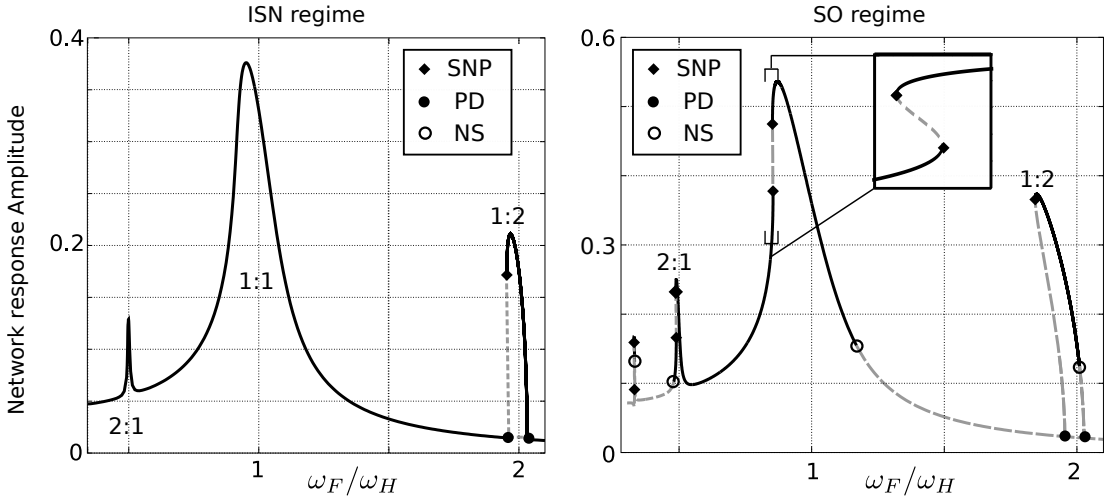

Figure 3: **Amplitude of the phase-locked solutions as function of the forcing frequency.** Left: Plot of the amplitude of the PL solutions for the same network as in Figure 2 in the ISN regime; parameters are $\epsilon = 0.07$, $\theta_E^{(0)} = 0$ and $\theta_I^{(0)} = -0.647$ ($\theta_{I,Hopf}^{(0)} = -0.647759$). Right: Amplitude plot for parameters of the forcing current in the SO regime: $\epsilon = 0.11$, $\theta_E^{(0)} = 2$ and $\theta_I^{(0)} = 1.5874$ ($\theta_{I,Hopf}^{(0)} = 1.595384$). Black lines are stable, dashed gray lines are unstable. Saddle Node of Periodic solution (SNP). Neimark-Sacker bifurcation (NS). Period Doubling bifurcation (PD).

bifurcation (Arnold 1983; Gambaudo, J. M. 1985; Zhang 2011). The dynamics of the forced network response amplitude close to the $k : l$ resonance is (Elphick 1987):

$$\dot{z} = z\left(a\delta\theta_I^{(0)} + c_1 + \imath\delta\omega - b|z|^2\right) + c_2\bar{z}^{l-1} + h.o.t. \tag{6}$$

where $\delta\omega = \omega_H - \frac{k}{l}\omega_F$ is the detuning parameter and

$$(E(t), I(t)) = (E^f, I^f) + z(t)e^{\imath\omega_H t}\zeta + \bar{z}(t)e^{-\imath\omega_H t}\bar{\zeta} + \Psi(z(t), \bar{z}(t), t) \tag{7}$$

where $t \to \Psi(\cdot, \cdot, t)$ is $\frac{2\pi}{\omega_F}$-periodic (see the Appendix A for an explanation) and represents a polynomials of order at least 2 whose contribution is neglectible because

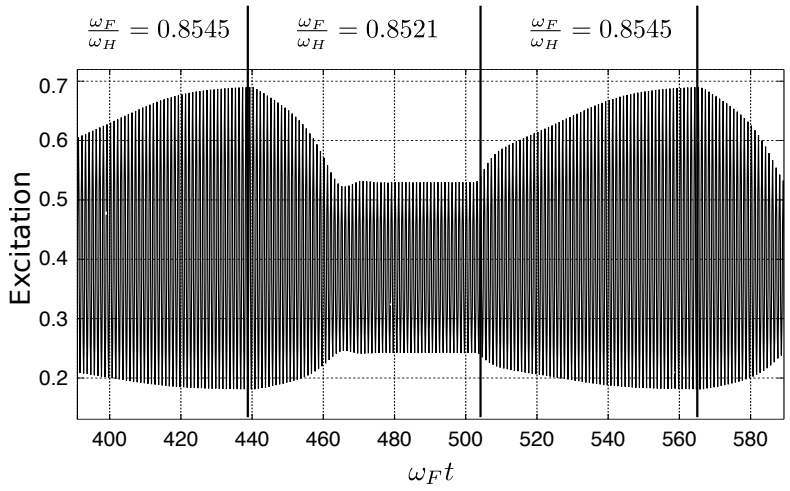

Figure 4: **Example of multi-stable response.** Plot of the excitatory population response amplitude for ω_F close to $0.853\,\omega_H$. Note that ω_F is slowly modulated to show the change between the stable states in the multi-stability region of Figure 3 Right. The figure shows a jump between two PL solutions of different amplitudes.

$|z| << 1$ Note that the coefficients c_1, c_2 have to be computed as functions of the network parameters $\epsilon, \delta\omega$ (see Appendices) while the other coefficients are the same as in eq (4). The normal form (6) describes the network response amplitude z as a dynamical object.

We will focus on the resonances $1:1, 1:2, 2:1$ for which $l = 1, 1, 2$ and use the detuning parameter $\delta\omega$ as a small parameter. By definition, around each resonance peak, the resonance curve is approximated by the function $\delta\omega \to |z|$ where z is solution of $\dot{z} = 0$ in eq (6).

The resonance curve near the resonance $1:1$ have been partially characterized in (Zhang 2011) and can be quite complicated. However, in the ISN regime only two types of resonance curves are possible (they are shown in Figure 10). However, the resonance curve is of little use if the stability of the PL solution is not given (as in (Zhang 2011)).

We propose to fill the gap in the following analysis. Here are some important properties of the main resonances that we prove in the following sections:

1. The maximum of the $1:1$ peak is not centered on ω_H when $\Im(b) \neq 0$.

2. There is multi-stability (and hysteresis near the peaks $1:1, 2:1$) in the ISN regime if and only if the shear γ (see eq (5)) satisfies $|\gamma| > \sqrt{3}$. See next section and also (Zhang 2011) for a proof. An example of hysteresis is shown in Figure 4. If the forcing amplitude ϵ is too small, the multi-stable PL disappear.

3. If the forcing amplitude ϵ is large enough, the maximum M of the $1:1$ resonance peak satisfies $\epsilon^{1/3}/2^{1/6} < M\frac{|\Re b|^{1/3}}{|\tilde{c}_2|} < \epsilon^{1/3}$ where $c_2 \stackrel{def}{=} \epsilon \cdot \tilde{c}_2$ (see (Golubitsky 2009)). As $\epsilon << 1$, it gives a very large amplification of the corresponding forcing frequency component. We plot the maximum of the resonance peaks $1:1, 1:2, 2:1$ in log-log coordinates in Figure 5.

4. No torus responses are possible in the ISN regime near the $1:1$ and $1:2$ resonances.

Given these properties, it is then straightforward to select a network that shows one of these features. For example, to have multi-stability, we need a large enough shear (see Figure 2 Right and Figure 3 Right). For torus solutions, the network should be in the SO regime.

3.4 Case of $1:1$ resonance

How do the different PL solutions interact? Can the torus solution exist together with multi-stable PL solutions? Are there any other behaviors? We will explore here these

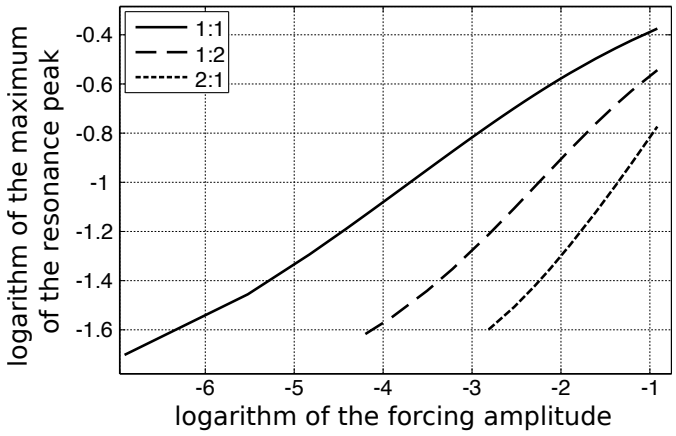

Figure 5: **Power law for the maximum of the resonance peaks.** Log of the resonance peak power for $1:1, 1:2, 2:1$ as function of the log of the forcing amplitude ϵ. Network parameters as in Figure 3 Right.

questions for the $1:1$ resonance. In the Appendix A, we computed the coefficients of the general normal form (6) around the resonance $1:1$:

$$\dot{z} = z\left(a\delta\theta_I^{(0)} + \imath(\omega_H - \omega_F) - b|z|^2\right) + \frac{\epsilon}{2}\langle DS\,\theta^{(1)}, \zeta^*\rangle. \tag{8}$$

where $DS\,\theta^{(1)} \stackrel{def}{=} (\theta_E^{(1)} S'(J_{EE}E^f + J_{EI}I^f + \theta_E^{(0)}), \theta_I^{(1)} S'(J_{IE}E^f + J_{II}I^f + \theta_I^{(0)}))$.

A complete understanding of the possible responses of the forced network near the resonance $1:1$ can be obtained by studying the dynamics generated by eq (8) as function of the parameters $\omega_F, \epsilon, \theta^{(0)}$. The problem is that there are at least three parameters $\delta\theta^{(0)}, \epsilon$ and $\delta\omega$, which makes the analysis difficult. However, eq (8) can be further simplified, using appropriate scaling $t = \alpha t', z = \beta Y$ (see Appendix D), into the following equation with 2 parameters:

$$\dot{Y} = Y\left(\epsilon_0 + \imath\tau - |Y|^2\right) e^{i\arg b} + \rho \tag{9}$$

where $Y \in \mathbb{C}, \rho \geq 0, \tau \in \mathbb{R}\ \rho > 0$and also (see appendices D,E):

$$\begin{cases} \epsilon_0 = \text{sign}\left(\delta\theta_I^{(0)}(\Re a + \gamma \Im a) + \gamma\delta\omega\right) = \pm 1 \\ \rho^{2/3} = \frac{\Im(b)}{\Re(a)\delta\theta_I^{(0)}}\left(\frac{|c_2|}{|b|}\right)^{2/3}\left(\frac{\epsilon_0}{\gamma} - \tau\right), \quad c_2 \stackrel{def}{=} \frac{\epsilon}{2}\langle DS\,\theta^{(1)}, \zeta^* \rangle \end{cases} \tag{10}$$

The complete bifurcation diagram of eq (9) can be found in (Arnold 1983; Gambaudo, J. M. 1985). The case $\epsilon_0 = -1$ is shown in Figure 6. It is very simple: torus solutions (*i.e.* Y is time-periodic) are possible if τ is sufficiently negative. The case $\epsilon_0 = 1, \gamma >$

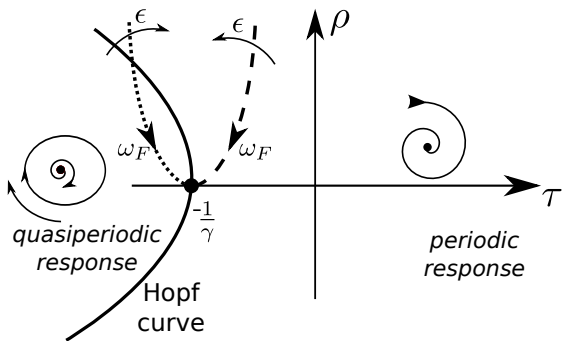

Figure 6: **Dynamics for the amplitude of the network response in the case $\epsilon_0 = -1$.** Bifurcation diagram of eq (8) in the plane (τ, ρ). The dashed curves are the resonance curves parametrized by the detuning $\delta\omega$ (dashed for the ISN regime, dotted for the SO regime). Adapted from (Gambaudo, J. M. 1985).

$1/\sqrt{3}$ is shown in Figure 7 and the case $\epsilon_0 = 1, 0 < \gamma < 1/\sqrt{3}$ can be found in (Gambaudo, J. M. 1985).

3.5 Description of the phase diagram in the case $\epsilon_0 = 1$

In this Figure 6, equilibria are marked with red dots and represent PL network responses whereas time-periodic solutions correspond to quasiperiodic network response (such as the one in Figure 8 Top). Two curves are particularly interesting in Figure 7:

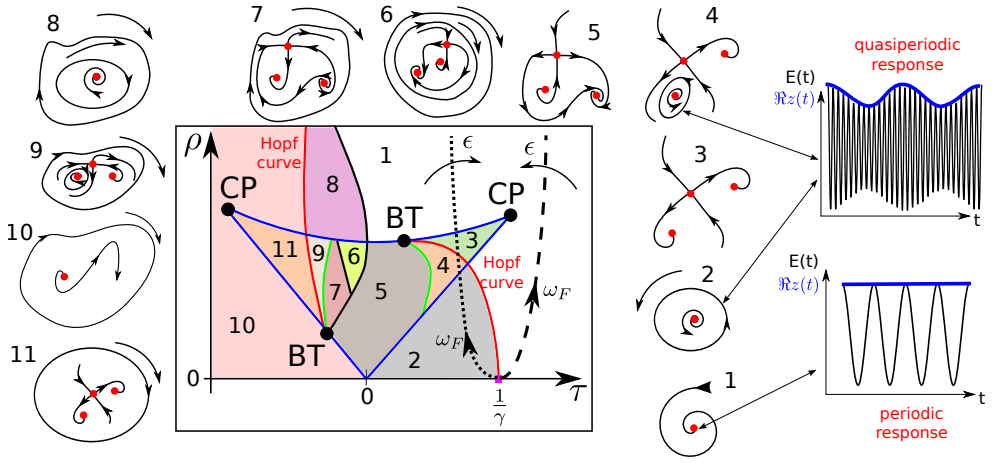

Figure 7: **Dynamics for the amplitude of the network response in the case** $\epsilon_0 = 1, \gamma > 1/\sqrt{3}$**.** Bifurcation diagram of eq (8) in the plane (τ, ρ). Red: curve of Hopf bifurcations. Blue: curve of Saddle-Node bifurcations. BT: Bogdanov-Takens bifurcation point. The dashed curves in black are the resonance curves parametrized by the detuning $\delta\omega$ (dashed for the ISN regime, dotted for the SO regime). The CP points have coordinates $\left(\frac{\pm 1}{\sqrt{3}}, \frac{2\sqrt{2}}{3\sqrt{3}}\right)$. The BT points have abscissa $\pm\frac{\Re b}{\Im b+2}$. (Adapted from (Gambaudo, J. M. 1985)). On the right, we show the link between the dynamics of the amplitude $z(t)$ (or $Y(t)$) and $E(t)$.

the first is the curve of Saddle-Node bifurcations (blue), which signals the appearance/disappearance of equilibria (marked as red dots) and the second is the Hopf bifurcation curve (red), which signal the appearance/disappearance of periodic orbits. The Saddle-Node curves give the parameter regions corresponding to multi-stable PL (such as phases diagram number 3 and 11) already mentioned in the previous section.

Hence, between the phase diagrams 3 and 4, a torus response is created by a Hopf bifurcation. The period of the response amplitude increases without bound as the parameters go from the phase diagram 4 to 5 (or 11 to 9) to the homoclinic bifurcation

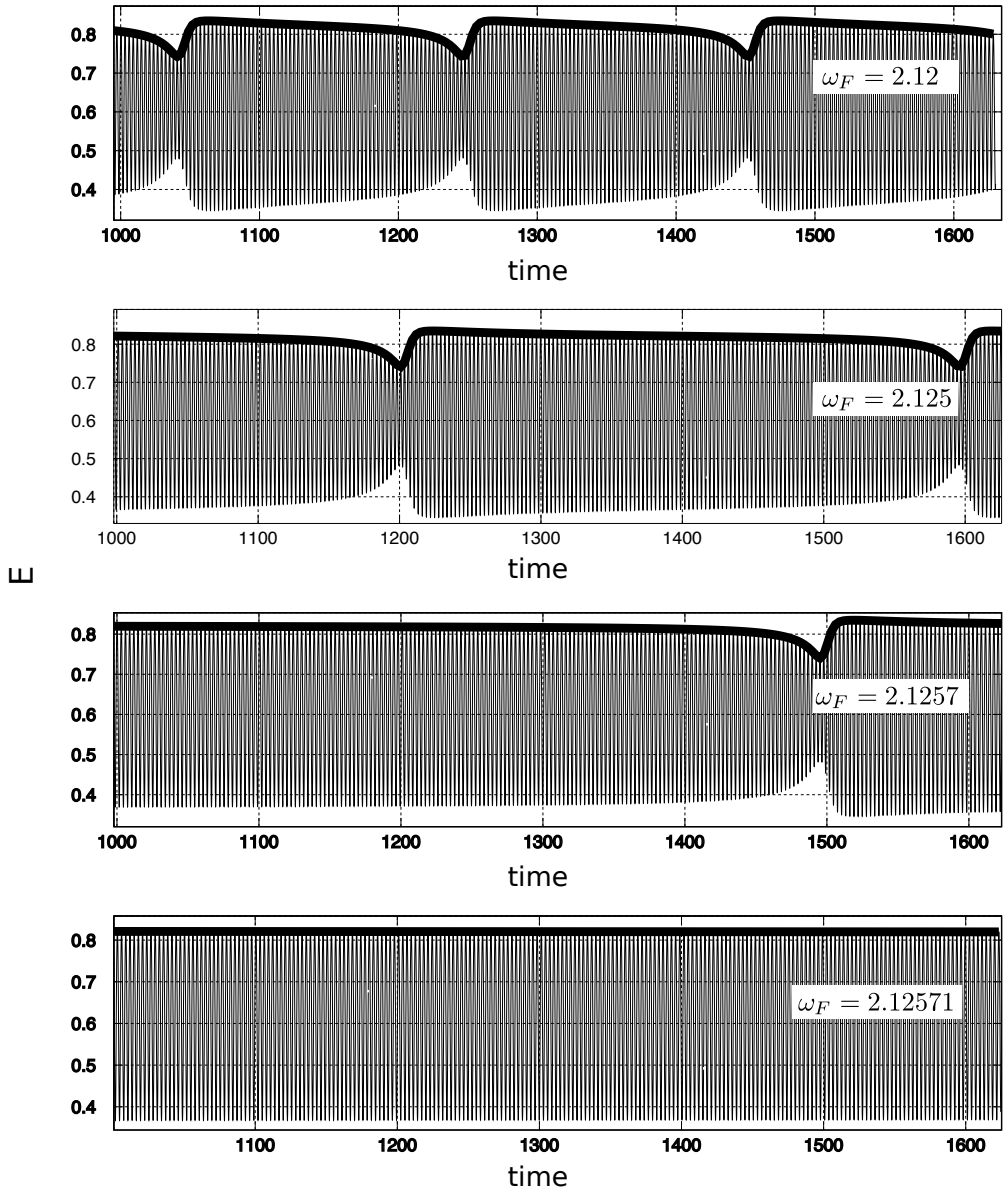

Figure 8: **Example of convergence to a homoclinic response.** Plot of the excitatory response for different forcing frequencies. The forcing parameters are such that the dynamics is close to the homoclinic curve. Different parameters from Figure 3 Right are $\theta_I^{(0)} = 0.824174, \epsilon = 0.05$.

curve. An example of such phenomenon of a homoclinic response is shown in Figure 8.

Remark 1. *There are some effects that are not captured by the normal form analysis.*

Along the Hopf curves, the frequency ω_{amp} of the response amplitude tends to zero at the BT points and the frequency ω_{amp} can be such that $\frac{\omega_{amp}}{\omega_H}$ is rational leading to Arnold tongues and possibly strong resonances. The same resonances can occur when going from the Hopf curves to the homoclinic curves. Hence, in phase diagram 4 and 9, there is a "torus breakdown" (see (Kuznetsov 1998)), usually associated with chaotic behavior of eq (1) *in which the torus solution becomes highly irregular.*

3.5.1 Application to the study of the response

We now study the specific effects of the three parameters $\epsilon, \omega_F, \delta\theta^{(0)}$ on the response of the forced network. In the Appendix E, we show that the three parameters describe a curve given by eq (10)-2 in the plane (τ, ρ) which is parametrized by the detuning parameter $\delta\omega$. They are plotted in figures 7,6 using dashed curves of equation. Recall that the resonance curve is given by $RC : \delta\omega \to |z|$ where z is solution of $\dot{z} = 0$ in eq (8). It can be solved by taking some norm in eq (8). Using the equivalent equation (9), one sees that $RC(-\delta) = RC(\delta)$ if the shear is zero $\gamma = 0$. Computing the resonance curve amounts to computing the equilibria as function of the detuning. But we can also predict the dynamics corresponding to a particular value of the detuning. Indeed, when the detuning is varied, the couple (τ, ρ) describes a curve of equation (10)-2 in the bifurcation diagram which allows to predict the response of the forced network.

The two type of curves, depending on the network regime (ISN or SO), are shown in Figure 6 and Figure 7. When varying the forcing frequency (or the detuning), the value of $\epsilon_0 \overset{def}{=} \text{sign}\left(\delta\theta^{(0)}(\Re a + \gamma\Im a) + \gamma\left(\omega_H - \omega_F\right)\right)$ changes, which has the consequence of switching the possible response dynamics between Figure 6 and Figure 7.

More precisely, if $\omega_F > \omega_H + \frac{\delta\theta^{(0)}}{\gamma}(\Re a + \gamma \Im a)$, the possible dynamics correspond to the one of Figure 6 whereas if $\omega_F < \omega_H + \frac{\delta\theta^{(0)}}{\gamma}(\Re a + \gamma \Im a)$, then the possible dynamics correspond to the one of Figure 7.

We now examine the working regimes ISN/SO in more details.

3.5.2 The ISN regime

Recall that this case corresponds to $\Re(a\delta\theta^{(0)}) < 0$ which forces $\frac{\epsilon_0}{\gamma} \leq \tau$ from eq (10)-2. Using Figures 6-7, the resonance curve never crosses the Hopf bifurcation curve and the network cannot produce torus solutions (See Appendix C for proof). Also, if $\Re(a\delta\theta^{(0)}) \approx 0$, the resonance curve (dashed black) is almost vertical and intersects the Saddle-node bifurcation curve i.f.f. $\frac{1}{\gamma} < \tau_{CP} = \frac{1}{\sqrt{3}}$ *i.e.* $\gamma > \sqrt{3}$; that is, the condition given in (Zhang 2011) ensuring multistability. Indeed, in this case the resonance curve crosses the region labeled 3 in Figure 7 where 2 stable equilibria are present. The same occurs if we increase the shear $|\gamma|$. The reader can check that $|\gamma| > \sqrt{3}$ for Figure 3 Right using the numerical values of the shear given in Figure 2. Finally, if the forcing amplitude ϵ increases, the regime of multi-stable PL becomes larger (if $|\gamma| > \sqrt{3}$) because the curve will shift from phase diagram 1 to phase diagram 3 (see the effect of the forcing amplitude ϵ on the curve in Figure 7). As a consequence, the only possible dynamics in the ISN regime are the ones labeled 1 and 3 in Figure 7.

Rephrasing these facts, the forced ISN network can only produce periodic reponses and multistable periodic responses that we called PL solutions.

3.5.3 The SO regime

The SO regime gives rise to a richer behavior than the ISN regime because $\frac{\epsilon_0}{\gamma} \geq \tau$ using eq (10)-2. In particular, the resonance curve can cross the Hopf curve, which generates torus solutions as for example in regions 2 and 4 in Figure 7. Reducing the forcing amplitude ϵ yields more dynamical effects as the resonance curve passes through all parts of the phase diagrams in Figure 7. It is for example straightforward to select an amplitude ϵ that produces an almost homoclinic response (green curve in Figure 7) as in Figure 8, or multi-stability between PL and torus responses (for example phase diagram 6 of Figure 7), or large amplitude torus responses as in phase diagrams $10, 11$. In contrast to the ISN regime, increasing the forcing amplitude leads to simpler dynamics.

Rephrasing these facts, the SO regime can produce periodic responses, quasiperiodic responses or even stranger behaviors like the one in Figure 8. Hence, the resonance curve is not enough to describe the dynamics (see incomplete case in Figure 3 Right) and one needs to at least compute and plot the quasiperiodic responses. This will be done numerically in the last section of the Results.

3.6 Case of the $2:1$ resonance

The shape of the resonances for the case $1:1$ and $2:1$ are qualitatively similar (see equation 6) because $l = 1$ in both cases. In particular, a necessary and sufficient condition for the $2:1$ resonance curve to display multi-stability is (see study of the $1:1$ resonance):

$$|\gamma| > \sqrt{3}. \tag{11}$$

The dynamics are the same as in Figures 6, 7 albeit occurring in a much narrower parameter region.

3.7 Case of the $1:2$ resonance

This case is different from the $1:1$ and $2:1$ resonances. Let us write the network response $(E(t), I(t))$ around the basal activity (E^f, I^f) as

$$(E(t), I(t)) = (E^f, I^f) + z(t)e^{\imath\omega_H t}\zeta + \bar{z}(t)e^{-\imath\omega_H t}\bar{\zeta} + \Psi(z(t), \bar{z}(t), t) \qquad (12)$$

where $t \to \Psi(\cdot, \cdot, t)$ is $\frac{2\pi}{\omega_F}$-periodic (see the Appendix A for an explanation) and represents a polynomials of order at least 2 whose contribution is neglectible because $|z| << 1$. The dynamics of the amplitude around the $1:2$ peak is governed by:

$$\dot{z} = z\left(a\delta\theta_I^{(0)} + \imath(\omega_H - \omega_F/2) - b|z|^2\right) + c_2\bar{z} \qquad (13)$$

where c_2 is proportional to the forcing amplitude ϵ (see the Appendix B). Unlike the previous cases, $z = 0$ is solution of this equation corresponding to the network response $(E(t), I(t)) = (E^f, I^f) + \Psi(0, 0, t)$, *i.e.* the response frequency is ω_F. On the other hand, the non-trivial constant solutions in z correspond to PL responses at frequency ω_H *i.e.* at half the forcing frequency from eq. (12). Thus, the PL solution undergoes a period doubling bifurcation around $\omega_F \approx 2\omega_H$ (see Figure 3).

The shape of the $1:2$ resonance peak can be found by solving $\dot{z} = 0$ in the previous equation, which leads to a quadratic equation in $|z|^3$ (see Appendix F). It always has the qualitative shape shown in Figure 3. In the Appendices F and G, we prove the following properties concerning the $1:2$ peak:

1. The 1:2 resonance peak exists only if the forcing amplitude is large enough: $|c_2| > \left|\Re a\delta\theta_I^{(0)}\right|$.

2. The width W of the peak scales linearly with the forcing amplitude $W \sim \epsilon$.

3. The height H of the peak scales linearly with the forcing amplitude $H \sim \epsilon$.

4. In the ISN regime, no quasiperiodic network response are possible.

We do not show all the possible responses as for the 1:1 peak due to a lack of space. However, all of the responses in the ISN regime are listed in the Appendix G. Reprased differently, the $1:2$ shows the remarkable feature that when the ISN is forced at frequency $\approx 2\omega_H$, it responds with a periodic response with frequency ω_H. This could explain why this peak was not seen in (Cardin 2009) for example.

3.8 Completion of the resonance curves in the SO regime

Our goal is now to complete the resonance curves (see Figure 3 Right) in the SO regime by computing the torus solutions amplitudes. To this end, we use the software Knut (see (Schilder 2005)) to compute the torus solutions emerging from the Hopf bifurcations for eq (6). The torus solutions have two intrinsic frequencies ω_F, ω_{app}, which generates the toroidal dynamics. When the *rotation number* ω_{app}/ω_F is rational, the torus becomes a periodic solution: this happens at the tip of the Arnold tongues. In Figure 9, we plot the PL amplitude and the torus amplitude as functions of the forcing frequency ω_F. An example of torus response is shown in Figure 9 Bottom Left. A PL response is shown in Figure 9 Top Left. A PL solution (close to the peak $1:2$) with frequency ω_H and forcing frequency $2\omega_H$ is shown in Figure 9 Bottom Right: this is

the period-doubling phenomenon that we studied earlier. Finally, we have also plotted,

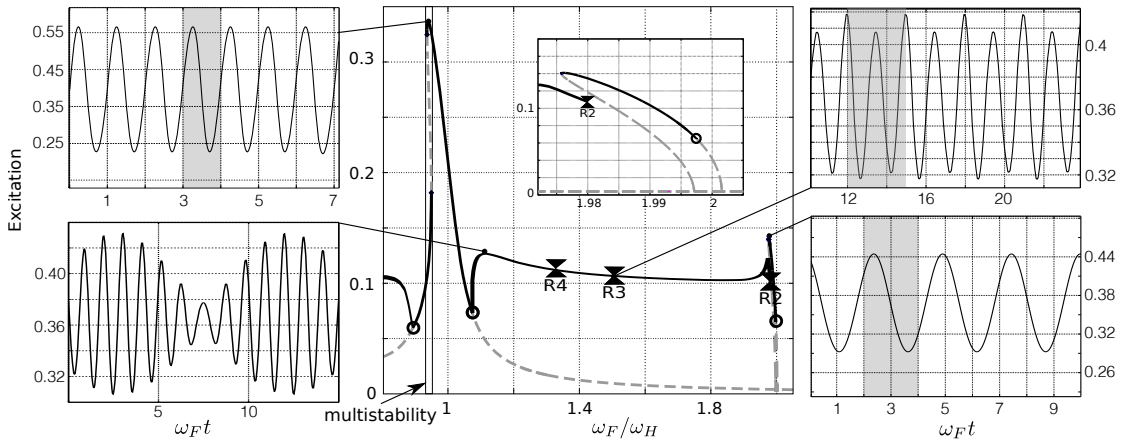

Figure 9: **Example of resonance curve in the SO regime.** Plot of the amplitude of the response as function of forcing frequency. Gray box shows one period of a periodic response. See text for further explanation. Parameters: $\epsilon = 0.01, \delta\theta^{(0)} = -0.0018$. Same network as in Figure 2. The torus solution is continued until the resonance R2 where the continuation fails. (Computed with Auto07p and Knut.)

with triangles, points where the rotation number is $\frac{1}{4}$ (labeled $R4$), $\frac{1}{3}$ (labeled $R3$) and $\frac{1}{2}$ (labeled $R2$). An example of a PL solution with frequency $\omega_F/3$ is shown in Figure 9 Bottom Left. This solution is very unstable and requires careful adjustment of the forcing frequency otherwise a torus solution appears.

4 Discussion

We have analyzed networks regimes that are important for understanding phase-amplitude coupling, which is relevant for communication between the hippocampus and the entorhinal cortex for example (Jensen 2007; Igarashi 2014). More precisely, we restricted our analysis to the periodic forcing of a specific class of inhibition stabilized E-I net-

works, working close to a Hopf bifurcation. The results apply to a mean field description of population of neurons and as such, most of our results should carry over to spiking neural networks in an ISN regime. Also, the results are insensitive to synaptic delays (Roxin 2005) as long as the network is close to a Hopf bifurcation.

Let us summarize some of our results and give predictions. We first have shown that the ISNs require the tuning of an E-I network close to a Hopf bifurcation effectively acting as a Stuart-Landau oscillators. We have shown that the periodic forcing of an E-I network, working close to a Hopf bifurcation, can lead to interesting phenomena that depend mainly on the value of the shear γ and whether or not the network is tuned to the ISN regime. In short, the ISN regime can only produce phase-locked solutions and hysteresis of phase-locked solutions when periodically forced. In contrast, networks that support sustained oscillations (such as the ones induced by carbachol in (Akam 2012)) are likely to produce torus responses when periodically forced. The shear breaks the symmetry of the $1:1$ resonance peak (see section 3.5.1), which makes periodic forcing of neural networks a flawed tool to determine the intrinsic gamma frequency (Akam 2012). An extreme example of this is shown in Figure 10 where the shear governs the birth of multistability.

We have examined the resonance curve and have shown, and predicted, that the main resonance peaks arise at $\frac{1}{2}, 1, 2$ times the network intrinsic frequency which reflects the large amplification of the input component located near these peaks (see (Ray 2011)). One interesting fact is that the resonance curves of the ISN networks are more isolated because they cannot produce torus responses (compare Figure 9 with Figure 3 Left). In particular, the ISN response to a broadband signal corresponds to a nonlinear and highly

selective filter at $1, 2, \frac{1}{2}$ times its intrinsic frequency ω_H. In comparison, the network with sustained oscillations will mix all frequency in a very complicated manner because of the torus responses.

We synthesize the results in Figure 10 for the ISN regime and for two different ranges of shears γ that lead to the two different classes of resonance curves. The largest the shear $|\gamma| > \sqrt{3}$, the largest the region of multistability. In the ISN regime, the network response frequency is the same as the forcing frequency except near the $1:2$ peak where it is half the forcing frequency. This period doubling phenomenon also works in the case of network that supports sustained oscillations. This constitute the first prediction. The second set of predictions concern the scaling of the different peaks as functions of the forcing amplitude ϵ as shown in Figure 10. As such, the resonance curve and the scaling of its peaks constitute an experimental indirect proof of an ISN working regime which can be tested using optogenetics experiments.

Most of these effects have been overlooked in studies focused on synchronization and phase locking (Hoppensteadt 1997; Izhikevich 2007) with notable exceptions (Vierling-Claassen 2009). The widely used theory of weakly-connected Hopf oscillations (WCHO) presented in (Hoppensteadt 1997) ignores resonance effects (Theorem 5.10) and only considers phase coupling. In our view, the resonant normal form is the one that should be perturbed using the detuning $\delta\omega$ when considering weakly connected oscillators, not the Hopf normal form used in (Hoppensteadt 1997). In particular the normal form for the external forcing of WCHO (Hoppensteadt 1997)[Theorem 5.8] leads to the incorrect conclusion that the resonant frequency only affects linear terms (see eq (6)).

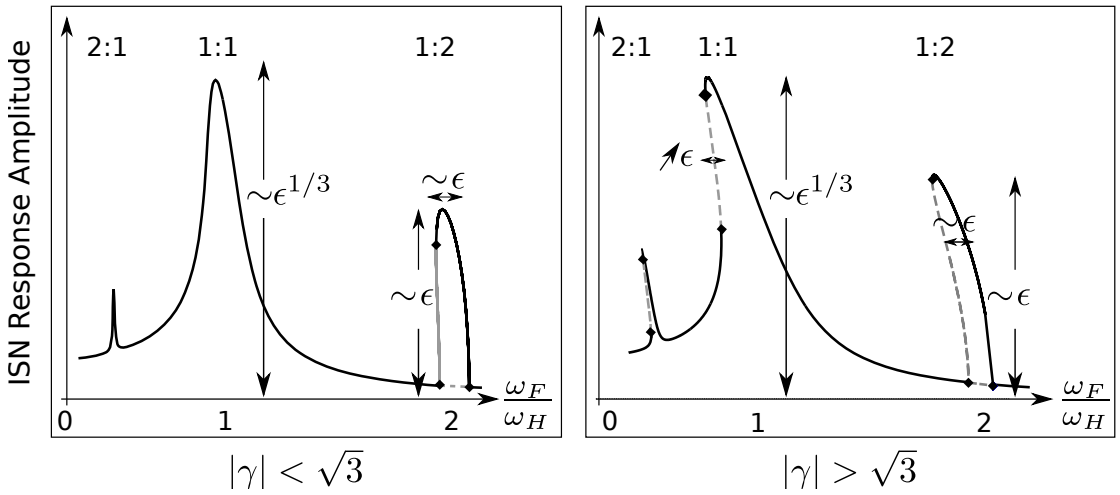

Figure 10: **Plot of the resonance curves in the ISN regime for two different shears γ.** The scaling of the width and amplitude of the peaks is indicated as function of the forcing amplitude ϵ. The domain of multistability for $|\gamma| > \sqrt{3}$ is a decreasing function of ϵ but an increasing function of γ. The amplitude of the $1:1$ peak does not scale exactly as $\epsilon^{1/3}$ as indicated. For more details, see text and appendix F.

In a more recent study (Ostojic 2008), the second resonance peak was missed because the authors consider an ansatz for the response at frequency $2\omega_H$ when the network is forced at $2\omega_H$, whereas the maximum response amplitude occurs at frequency ω_F based on our results. It was also overlooked in (Cardin 2009) because the authors only extracted from the network response, the frequency component around the forcing frequency ω_F, thereby possibly throwing away the main frequency component around $\omega_F/2$ when the forcing frequency is at twice the gamma-peak frequency.

Periodic forcing of a supercritical Hopf bifurcation for single neuron dynamics is rare and consequently has not been studied. Indeed, class II neurons work close to a subcritical Hopf bifurcation with a Fold on the limit cycle branch (Izhikevich 2007). This suggests that periodic forcing of the Generalized Hopf bifurcation (also called a

Bautin bifurcation) is relevant for resonance effects in class II neurons and should be more closely examined.

A central hypothesis of this work is that of an ISN. We have shown that this requires the network to be tuned close to a Hopf bifurcation. Hence, all the results presented here are indirected proof of this working regime if ever found in experiments. The normal form method (Haragus 2010) can be applied to study networks close to other local bifurcations like the Bogdanov-Takens for example.

Another assumption of the model is that of periodic forcing. A generalization would be to the case of quasiperiodic forcing which seems more relevant to the real world. We expect the general form the resonance curves to remain if there is dominant frequency in the forcing (Saleh 2010).

As suggested in (Golubitsky 2009), feedforward chains of n ISN networks are highly selective to the forcing frequency as the maximum of the $1:1$ peak, for the n-th network, is $\epsilon^{1/3^n}$ (other peaks have similar power laws). Thus, these feedforward chains would be very useful for extracting frequency components of noisy inputs by working as nonlinear filters, and would be able, at the same time, to demultiplex the main components of the input. We plan to examine this effect in feedback networks.

We also plan to explore the effects of adding noise to the periodic forcing, which should exhibit stochastic resonance phenomena. Indeed, one of the first studies of stochastic resonance (Benzi 1981) considered the periodic forcing of a pitchfork bifurcation with noise perturbation, which led to multi-stability of PL solutions. When multi-stable PL solutions are perturbed with noise, they exhibit stochastic resonance. Similarly, the periodic forcing of the Hopf bifurcation with large enough shear should

also exhibit multi-stability, which is the main ingredient in (Benzi 1981).

Acknowledgment

We would like to thank Frank Schilder and Robert Szalai for their help in computing the torus solutions. We warmly thank Antonio Pinto-Duarte for his valuable comments on the manuscript.

This work was partially supported by the European Union Seventh Framework Programme (FP7/2007-2013) under grant agreement no. 269921 (BrainScaleS), no. 318723 (Mathemacs), and by the ERC advanced grant NerVi no. 227747 and by the Human Brain Project (HBP).

Notation for hermitian scalar products for vectors and functions: $\langle V, W\rangle \stackrel{def}{=} V_1\overline{W_1} + V_2\overline{W_2}$ and $\langle f, g\rangle_{per,\tau} \stackrel{def}{=} \frac{1}{\tau}\int_o^\tau \langle f(t), g(t)\rangle dt$.

We call ζ and ζ^* the eigenvector of the Jacobian and the Jacobian adjoint at the equilibrium, respectively, for the eigenvalues $\imath\omega_H$ and $-\imath\omega_H$ with the normalization $\langle \zeta, \zeta^*\rangle = 1$.

A Normal form computation of the 1:1 resonance

Proposition A.1. *The normal form of eq* (1) *for the* $1:1$ *resonance is*

$$\dot{z} = z\left(a\delta\theta^{(0)} + \imath(\omega_H - \omega_F) - b|z|^2\right) + c_2\epsilon$$

where $c_2 = \frac{1}{2}\langle \theta^{(1)} dS(V^f + \theta^{(0)}), \zeta^*\rangle$ *and* b *is defined in eq* (4)*.*

Proof. In order to apply the result (Haragus 2010)[III.5.2], we need the forcing frequency to be constant. Hence, we start by rescaling the time variable $s \stackrel{def}{=} \omega_F t$, which yields:

$$\begin{aligned}\frac{d}{ds}V &= \frac{1}{\omega_F}\left[-V + S(\mathbf{J}\cdot V + \theta^{(0)} + \epsilon\theta^{(1)}\cos(s))\right] \\ &= \frac{1-\omega}{\omega_H}\left[-V + S(\mathbf{J}\cdot V + \theta^{(0)} + \epsilon\theta^{(1)}\cos(s))\right].\end{aligned}$$

The bifurcation parameters are $\mu = (\theta^{(0)}, \epsilon, \omega)$ and the bifurcation point is $\mu_c = (\theta_H^{(0)}, 0, 0)$, $V = V^f$. It follows that the Hopf frequency is 1 at the bifurcation point $\mu = \mu_c$. We write $V(s) = V^f + v_0(s) + \Psi(v_0(s); \theta^{(0)}, \epsilon, \omega, s)$ where $\Psi(0; \theta_H^{(0)}, 0, 0, s) = 0$, $D_1\Psi(0; \theta_H^{(0)}, 0, 0, s) = 0$ and Ψ is 1-periodic in s. From (Haragus 2010)[III.5.2], we

have $v_0(s) = A(s)\zeta + c.c.$ and:

$$\dot{A} = \imath A + a(\theta^{(0)}, \epsilon)A + c(\theta^{(0)}, \epsilon)e^{\imath s} + e(\theta_H^{(0)}, 0)A^2 e^{-\imath s} + f(\theta_H^{(0)}, 0)\bar{A}^2 e^{3\imath s} + b(\theta_H^{(0)}, 0)|A|^2 A + g(\theta_H^{(0)}, 0)A^3 e^{-2\imath s} + h(\theta_H^{(0)}, 0)\bar{A}^3 e^{4\imath s} + j(\theta_H^{(0)}, 0)\bar{A}|A|^2 e^{2\imath s}.$$

As the right-hand side $G(V; \theta^{(0)}, \epsilon, t)$ of $\frac{d}{dt}V = \left[-V + S(J \cdot V + \theta^{(0)} + \epsilon\theta^{(1)} \cos(\omega_F t))\right]$ satisfies $\partial_t G(V; \theta_H^{(0)}, 0, t) = 0$, all the coefficients with an exponential factor vanish at $\mu = \mu_c$ (see (Haragus 2010)[III.5.2,Remark 5.5]), hence to lowest order:

$$\dot{A} = \imath A + a(\theta^{(0)}, \epsilon)A + c(\theta^{(0)}, \epsilon)e^{\imath s} + b(\theta_H^{(0)}, 0)|A|^2 A.$$

Finally, writing $A(s) = z(s)e^{\imath s}$, we find:

$$\dot{z} = \left(a(\theta^{(0)}, \epsilon) + b(\theta_H^{(0)}, 0)|z|^2\right) z + c(\theta^{(0)}, \epsilon).$$

We now compute the coefficients $a(\theta^{(0)}, \epsilon), c(\theta^{(0)}, \epsilon)$ as a linear expression of the parameters $(\theta^{(0)}, \epsilon)$ and also the coefficient b. First, Taylor expand the function Ψ:

$$\Psi(v_0; \mu) = \sum_{l_1 + l_2 + r > 1} A^{l_1} \bar{A}^{l_2} \mu^r \tilde{\Psi}_{l_1, l_2, r}.$$

Using the equation (5.5) in (Haragus 2010)[III.5] for the normal form change of variable Ψ and Fourier series, we find:

$$\begin{cases} a(\theta_H^{(0)}, 0) &= \langle G_{11}(\zeta) + 2G_{20}(\zeta, \Psi_{001}), \zeta^* \rangle_{per,1} \\ c(\theta_H^{(0)}, 0) &= \langle G_{01}(\zeta), e^{-\imath s}\zeta^* \rangle_{per,1} \\ b(\theta_H^{(0)}, 0) &= \langle 2G_{20}(\zeta, \Psi_{110}) + 2G_{20}(\zeta, \bar{\Psi}_{200}) + 3G_{30}(\zeta, \zeta, \bar{\zeta}), \zeta^* \rangle_{per,1} \end{cases} \tag{14}$$

where $G_{ij} \overset{def}{=} \frac{\partial^{i+j} G}{\partial^i V \partial^j \mu}$. It is straightforward to check that the expression of b is the same as for the case of a regular Hopf bifurcation without forcing (Kuznetsov 1998;

Haragus 2010). Hence, we have

$$b(\theta_H^{(0)}, 0) = \frac{b}{\omega_H}.$$

Let $G_{01} = \frac{d\epsilon}{\omega_H} DS\ \theta^{(1)} \cos(s) + \frac{d\theta^{(0)}}{\omega_H} DS$ with $DS \overset{def}{=} DS(\mathbf{J} \cdot V^f + \theta_H^{(0)})$. Indeed, the derivative *w.r.t.* ω vanishes at $V = V^f,\ \mu = \mu_c$, and this gives the coefficient:

$$c(\theta_H^{(0)}, 0) = \frac{\epsilon}{2\omega_H} \langle DS\ \theta^{(1)}, \zeta^* \rangle. \tag{15}$$

Let us focus now on the linear coefficient $a(\theta_H^{(0)}, 0)A$. We start with the expression of G_{20}:

$$G_{20}(U_1, U_2) = D^{(2)}S(\mathbf{J} \cdot V^f + \theta_H^{(0)})(\mathbf{J} \cdot U_1)(\mathbf{J} \cdot U_2)$$

which is time s independent. The equation for Ψ_{001} is:

$$\frac{d}{ds}\Psi_{001} - \mathbf{L}\Psi_{001} = G_{01}$$

where $\mathbf{L}$ is the Jacobian at $V = V^f$. Using Fourier series $G_{01} = \sum_{n=-\infty}^{\infty} G_{01}^{(n)} e^{\imath n s}$ and $\Psi_{001} = \sum_{n=-\infty}^{\infty} \Psi_{001}^{(n)} e^{\imath n s}$, we find:

$$(\imath n - \mathbf{L})\ \Psi_{001}^{(n)} = G_{01}^{(n)},\ \forall n \in \mathbb{Z}$$

From the expression of G_{20} and the scalar product $\langle G_{20}(\zeta, \Psi_{001}), \zeta^* \rangle_{per,1}$ in the expression of $a(\theta_H^{(0)}, 0)$, it appears that only the term $\langle G_{20}(\zeta, \Psi_{001}^{(0)}), \zeta^* \rangle_{per,1}$ is non vanishing: this gives $-\langle G_{20}(\zeta, \mathbf{L}^{-1} G_{01}^{(0)}), \zeta^* \rangle_{per,1}$. Also from the expression of G_{01}:

$$G_{11} = -\frac{d\omega}{\omega_H}\mathbf{L} + \frac{d\theta^{(0)}}{\omega_H} D^{(2)}S\mathbf{J} + \frac{d\epsilon}{\omega_H}\theta^{(1)}\cos(s) D^{(2)}S\mathbf{J},\ D^{(2)}S \overset{def}{=} D^{(2)}S(\mathbf{J} \cdot V^f + \theta_H^{(0)}).$$

This allows us to find an expression for $a(\theta_H^{(0)}, 0)$ using $\langle \mathbf{L}\zeta, \zeta^* \rangle_\tau = \imath\omega_H$:

$$a(\theta_H^{(0)}, 0) = -i\omega + \frac{d\theta^{(0)}}{\omega_H} \left(\langle D^{(2)}S\mathbf{J} \cdot \zeta - 2G_{20}(\zeta, \mathbf{L}^{-1} G_{01}^{(0)}), \zeta^* \rangle_{per,1} \right).$$

The second term is the same as for the case of no forcing (Kuznetsov 1998; Haragus 2010), hence we find:

$$a(\theta_H^{(0)}, 0) = -i\omega + \frac{d\theta^{(0)}}{\omega_H} a.$$

where a is defined in eq (4). To sum up, we have found that:

$$\frac{d}{ds}A = \left(\imath(1-\omega) + \frac{d\theta^{(0)}}{\omega_H} a\right) A + \frac{b}{\omega_H}|A|^2 A + \frac{\epsilon}{2\omega_H}\langle DS\,\theta^{(1)}, \zeta^*\rangle e^{\imath s}$$

or

$$\frac{d}{ds}z = \left(-\imath\omega + \frac{d\theta^{(0)}}{\omega_H} a\right) z + \frac{b}{\omega_H}|z|^2 z + \frac{\epsilon}{2\omega_H}\langle DS\,\theta^{(1)}, \zeta^*\rangle.$$

Coming back to the original time $t = s\omega_F = \frac{\omega_H}{1-\omega} s$, we find:

$$\frac{d}{dt}z = \left(-\imath\omega\omega_F + \frac{d\theta^{(0)}}{1-\omega} a\right) z + \frac{b}{1-\omega}|z|^2 z + \frac{\epsilon}{2(1-\omega)}\langle DS\,\theta^{(1)}, \zeta^*\rangle,$$

which gives

$$\frac{d}{dt}z = \left(\imath(\omega_H - \omega_F) + d\theta^{(0)} a\right) z + b|z|^2 z + \frac{\epsilon}{2}\langle DS\,\theta^{(1)}, \zeta^*\rangle.$$

B Normal form computation of the 1:2 resonance

Proposition B.1. *The normal form for the* $1:2$ *resonance is*

$$\dot{z} = z\left(a\delta\theta^{(0)} + \imath(\omega_H - \omega_F/2) - b|z|^2\right) + c_2\bar{z}$$

where $c_2 = \frac{\epsilon}{2}\langle D^{(2)} S\theta^{(1)}\mathbf{J}\cdot\zeta + 2G_{20}(\zeta, (2\imath\omega_H - \mathbf{L})^{-1} DS\theta^{(1)}), \zeta^*\rangle$ *and* b *is defined in eq* (4).

Proof. The proof in Appendix A shows that we only need to consider the case $\omega_F = 2\omega_H$ and incorporate the detuning parameter ω as a linear term. Hence:

$$c_2 = \epsilon\langle G_{11}(\zeta) + 2G_{20}(\zeta, \Psi_{001}), e^{-2\imath\omega_H t}\zeta^*\rangle_{per,2\pi/\omega_F}$$

which gives

$$c_2 = \frac{1}{2}\epsilon\langle D^{(2)}S\theta^{(1)}J\cdot\zeta + 2G_{20}(\zeta, \Psi^{(1)}_{001}), \zeta^*\rangle$$

where $\Psi_{001} = \sum_n \Psi^{(n)}_{001}e^{2\imath\omega_H nt}$ and

$$c_2 = \frac{\epsilon}{2}\langle D^{(2)}S\theta^{(1)}J\cdot\zeta + 2G_{20}(\zeta, (2\imath\omega_H - \mathbf{L})^{-1}DS\theta^{(1)}), \zeta^*\rangle.$$

C Hopf bifurcation curve near the $1:1$ resonance

Lemma C.1. *When $\Re(a)\delta\theta^{(0)}_I < 0$, the resonance curve does not intersect the Hopf bifurcation curve.*

Proof. In order to simplify, let us assume $\Re b = 1$ and write the $1:1$ normal form (after a scaling in z to transform $c_2 \to |c_2|$)

$$\dot{z} = z\left(\lambda + i\omega - (1+i\gamma)|z|^2\right) + |c_2|$$

where we have written $\omega = \delta\omega + \Im a\delta\theta^{(0)}_I$, $\lambda = \Re a\delta\theta^{(0)}_I$ and γ is the shear. The Hopf bifurcation curve is computed using two conditions (Kuznetsov 1998) regarding the Jacobian $\mathbf{L}$ of the above dynamical system: $\det(\mathbf{L}) > 0, tr(\mathbf{L}) = 0$, which satisfies:

$$\frac{1}{2}\omega^2\lambda - \frac{1}{2}\lambda^2\gamma\omega + \frac{1}{8}(\gamma^2+1)\lambda^3 - |c_2|^2 = 0.$$

There is a solution ω if and only if $\lambda(8|c_2|^2 - \lambda^3) > 0$. This condition is not satisfied when $\lambda < 0$.

D Simplification of the 1:1 normal form

Lemma D.1. *If $\Re b > 0, \Im b > 0$ and $\delta\theta_I^{(0)}(\Re a + \gamma\Im a) + \gamma\delta\omega \neq 0$ then the equation*

$\dot{z} = z(a\delta\theta_I^{(0)} + i\delta\omega - b|z|^2)z + c_2$ *is equivalent to the equation*

$$\dot{z} = z(\epsilon_0 + i\tau - |z|^2)ze^{i\arg(b)} + \rho \tag{16}$$

where $\epsilon_0 = sign\left(\delta\theta_I^{(0)}(\Re a + \gamma\Im a) + \gamma\delta\omega\right)$, $\tau = \frac{\delta\omega + \delta\theta_I^{(0)}(\Im a - \gamma\Re a)}{|\gamma\delta\omega + \delta\theta_I^{(0)}(\Re a + \gamma\Im a)|}$ *and* $\rho = \frac{|c_2|\cdot|b|^2}{|\Re b|^{3/2}\cdot|(\Re a + \gamma\Im a)\delta\theta_I^{(0)} + \gamma\delta\omega|^{3/2}}$.

Proof. For the scaling: $z \to ze^{-i\arg c_2}$, this implies $c_2 \to |c_2|$. For the scaling: $t \to Rt$ and $z \to Az$ with appropriate A, R, this implies $\epsilon_0 = sign\Re\frac{a\delta\theta_I^{(0)} + i\delta\omega}{b}$, $\tau = \Im\frac{a\delta\theta_I^{(0)} + i\delta\omega}{b}\left|\Re\frac{a\delta\theta_I^{(0)} + i\delta\omega}{b}\right|^{-1}$ and $\rho = \frac{|c_2|}{|b|\cdot\left|\Re\frac{a\delta\theta_I^{(0)} + i\delta\omega}{b}\right|^{3/2}}$.

Recall that $\cos\arg(b) > 0$ because the Hopf bifurcation is supercritical. Then: $\epsilon_0 = sign\Re\left(\frac{a\delta\theta_I^{(0)} + 1\delta\omega}{b}\right) = sign\left(\cos\arg(b)\frac{\delta\theta_I^{(0)}\Re a + \gamma\delta\theta_I^{(0)}\Im a + \gamma\delta\omega}{|b|(1+\gamma^2)}\right) = sign\left(\delta\theta_I^{(0)}(\Re a + \gamma\Im a) + \gamma\delta\omega\right)$.

Expressions for τ and ρ follow accordingly:

$\tau = \Im\left(\frac{a\delta\theta_I^{(0)} + 1\delta\omega}{b}\right)/\Re\left(\frac{a\delta\theta_I^{(0)} + 1\delta\omega}{b}\right)$, $\rho = |c_2|/|b| \cdot \left|\Re\frac{a\delta\theta_I^{(0)} + i\delta\omega}{b}\right|^{3/2}$.

E Equation of the resonance curve in the plane (τ, ρ)

Corollary E.0.1. *From the previous Appendix D the parameters satisfy:*

$$\rho^{2/3} = \frac{\Im(b)}{\Re(a)\delta\theta_I^{(0)}}\left(\frac{|c_2|}{|b|}\right)^{2/3}\left(\frac{\epsilon_0}{\gamma} - \tau\right), \quad c_2 \overset{def}{=} \frac{\epsilon}{2}\langle DS\,\theta_I^{(1)}, \zeta^*\rangle. \tag{17}$$

assuming that the Hopf bifurcation is supercritical, i.e. $\Re(b) > 0$.

Proof. We first compute $\frac{\epsilon_0}{\gamma} - \tau = \frac{\Re(a)\delta\theta_I^{(0)}\left(\gamma + \frac{1}{\gamma}\right)}{|\gamma\delta\omega + \delta\theta_I^{(0)}(\Re a + \gamma\Im a)|}$ and $\left(\frac{\rho}{|c_2|\cdot|b|^2}\right)^{2/3} = \frac{1}{|\Re b|\cdot|\gamma\delta\omega + \delta\theta_I^{(0)}(\Re a + \gamma\Im a)|}$ which gives

$$\frac{\epsilon_0}{\gamma} - \tau = \left(\frac{\rho|b|}{|c_2|}\right)^{2/3}\left[\Re(a)\delta\theta_I^{(0)}\right]\left(\gamma + \frac{1}{\gamma}\right)\frac{|\Re(b)|}{|b|^2} = \left(\frac{\rho|b|}{|c_2|}\right)^{2/3}\left[\Re(a)\delta\theta_I^{(0)}\right]\frac{\text{sign}(\Re b)}{\Im(b)}.$$

Using the fact that $\Re(b) > 0$ allows to conclude the proof.

F Properties of the PL solutions around the 1:2 resonance

Lemma F.1. *We show here that the 1:2 resonance peak has the following properties:*

1. *The peak exists if and only if* $|c_2|^2 > \left(\Re a\delta\theta_I^{(0)}\right)^2$*, i.e. if the forcing amplitude is large enough.*

2. *The width at its base is* $2\sqrt{||c_2|^2 - \lambda^2|}$*. Hence it scales as the amplitude* ϵ *since* c_2 *is proportional to the forcing amplitude.*

3. *Its height is* $|c_2| + \Re a\delta\theta_I^{(0)} > 0$*.*

Proof. Let us define: $\lambda \stackrel{def}{=} \Re a\delta\theta_I^{(0)}$ and $\omega \stackrel{def}{=} \Im a\delta\theta_I^{(0)} + \omega_H - \omega_F/2$. Using the scaling: $z \to ze^{-i\arg c_2/2}$, we can replace c_2 by its modulus. PL solutions are solutions to the equation:

$$z\left(a\delta\theta_I^{(0)} + \imath(\omega_H - \omega_F/2) - b|z|^2\right) + c_2\bar{z} = 0,$$

which gives $z = 0$ or $(1+\gamma^2)\,Y^2 - 2\,(\lambda + \omega\gamma)\,Y + (\lambda^2 - |c_2|^2 + \omega^2) = 0$ where $Y \stackrel{def}{=} \Re bX$ and $X \stackrel{def}{=} |z|^3$. The width at its base given by the difference of the ω such that $Y = 0$ is solution. These ω satisfy $\lambda^2 - |c_2|^2 + \omega^2$ which gives the width $2\sqrt{||c_2|^2 - \lambda^2|}$. It is only positive if $|c_2|^2 > \lambda^2$. Hence, this proves 1. and 2.

From the Implicit function theorem, the maximum Y_m of Y as function of ω occurs for a value ω_m such that $\omega_m = \gamma Y_m$. Result 3 follows by inserting this last expression in the quadratic equation: $Y_m = \lambda + |c_2| > 0$.

G Dynamics around the 1:2 resonance peak

We characterize here the dynamics of the 1:2 resonance in the ISN regime, $\Re a\delta\theta_I^{(0)} < 0$. We show that no torus solutions are possible and that there are 1, 3 or 5 PL solutions.

Lemma G.1. *In the ISN regime, i.e. when $\Re a\delta\theta_I^{(0)} < 0$, no torus solutions are possible. There are 1, 3 or 5 PL solutions.*

Proof. We first simplify the 1:2 normal form using successive re-scalings. Using the scaling $z \to ze^{-i\arg c_2/2}$, we can replace c_2 by its modulus. Then, using a real scaling $z \to z/\sqrt{|b|}$, we can assume $|b| = 1$. Hence, we can assume that we have $\dot{z} = z(\left(a\delta\theta_I^{(0)} + i(\omega_H - \omega_F/2)\right) e^{-i\arg b} - |z^2|)e^{i\arg b} + |c_2|\bar{z}$. Finally, using the scalings $z \to z/\sqrt{|c_2|}$ and $t \to |c_2|t$, we arrive at the equation

$$\dot{z} = z(\sigma + i\tau - |z^2|)e^{i\arg b} + \bar{z}$$

where $\sigma + i\tau = \left(a\delta\theta_I^{(0)} + i(\omega_H - \omega_F/2)\right) e^{-i\arg b}/|c_2|$. A resonance curve parametrized by ω_F describes a line in the plane (τ, σ) given by:

$$\tau = \gamma\sigma + \left(1 + \gamma^2\right) \Re(a\delta\theta_I^{(0)}) \frac{\Re b}{|b|^2}$$

Hence, in the ISN regime ($\Re a\delta\theta_I^{(0)} < 0$), this line is below the Hopf curve (H), $\tau = \gamma\sigma$, in the parameter plane (see (Gambaudo, J. M. 1985)[Figure 25]). This shows that the ISN regime can only produce the phase diagrams 1., 5. or 4. in (Gambaudo, J. M. 1985)[Figure 25] all of which are composed solely of fixed points.

References

[Akam 2010] Thomas Akam and Dimitri M. Kullmann. *Oscillations and Filtering Networks Support Flexible Routing of Information*. Neuron, vol. 67, no. 2, pages 308–320, July 2010.

[Akam 2012] Thomas Akam, Iris Oren, Laura Mantoan, Emily Ferenczi and Dimitri M Kullmann. *Oscillatory dynamics in the hippocampus support dentate gyrus-CA3 coupling*. Nature Neuroscience, vol. 15, no. 5, pages 763–768, April 2012.

[Arnold 1983] V. I. Arnold. Geometrical methods in the theory of ordinary differential equations. Springer–Verlag New York Inc., 1983.

[Aronson 1990] D.G. Aronson, B. Ermentrout and N. Kopell. *Amplitude response of coupled oscillators*. Physica D, vol. 41, page 403449, 1990.

[Bartos 2007] M. Bartos, I. Vida and P. Jonas. *Synaptic mechanisms of synchronized gamma oscillations in inhibitory interneuron networks*. Nature Reviews Neuroscience, vol. 8, no. 1, page 4556, 2007.

[Benzi 1981] R Benzi, A Sutera and A Vulpiani. *The mechanism of stochastic resonance*. Journal of Physics A: Mathematical and General, vol. 14, no. 11, pages L453–L457, November 1981.

[Bichot 2005] Narcisse P. Bichot, Andrew F. Rossi and Robert Desimone. *Parallel and Serial Neural Mechanisms for Visual Search in Macaque Area V4*. Science, vol. 308, no. 5721, pages 529–534, April 2005. PMID: 15845848.

[Borisyuk 1992] R. M Borisyuk and A. B Kirillov. *Bifurcation analysis of a neural network model*. Biological Cybernetics, vol. 66, no. 4, page 319325, 1992.

[Borisyuk 1995] G. N Borisyuk, R. M Borisyuk, A. I Khibnik and D. Roose. *Dynamics and bifurcations of two coupled neural oscillators with different connection types*. Bulletin of mathematical biology, vol. 57, no. 6, page 809840, 1995.

[Buzsaki 2004] Gyrgy Buzsaki and Andreas Draguhn. *Neuronal Oscillations in Cortical Networks*. Science, vol. 304, no. 5679, pages 1926–1929, June 2004.

[Buzski 1995] Gyrgy Buzski and James J Chrobak. *Temporal structure in spatially organized neuronal ensembles: a role for interneuronal networks*. Current Opinion in Neurobiology, vol. 5, no. 4, pages 504–510, August 1995.

[Cardin 2009] Jessica A. Cardin, Marie Carln, Konstantinos Meletis, Ulf Knoblich, Feng Zhang, Karl Deisseroth, Li-Huei Tsai and Christopher I. Moore. *Driving fast-spiking cells induces gamma rhythm and controls sensory responses*. Nature, vol. 459, no. 7247, pages 663–667, June 2009.

[Colgin 2009] Laura Lee Colgin, Tobias Denninger, Marianne Fyhn, Torkel Hafting, Tora Bonnevie, Ole Jensen, May-Britt Moser and Edvard I. Moser. *Frequency of gamma oscillations routes flow of information in the hippocampus*. Nature, vol. 462, no. 7271, pages 353–357, November 2009.

[Decker 2012] R. Decker and V. W. Noonburg. *A Periodically Forced WilsonCowan*

System with Multiple Attractors. SIAM Journal on Mathematical Analysis, vol. 44, no. 2, pages 887–905, January 2012.

[Elphick 1987] C. Elphick, G. Iooss and E. Tirapegui. *Normal form reduction for time-periodically driven differential equations*. Physics Letters A, vol. 120, no. 9, pages 459–463, March 1987.

[Ermentrout 1981] G. B Ermentrout. *n: m Phase-locking of weakly coupled oscillators*. Journal of Mathematical Biology, vol. 12, no. 3, page 327342, 1981.

[Ermentrout 2010] G. Bard Ermentrout and David Terman. Foundations of mathematical neuroscience. Interdisciplinary Applied Mathematics. Springer, 2010.

[Gambaudo, J. M. 1985] Gambaudo, J. M. *Perturbation of a hopf bifurcation by an external time-periodic forcing*. Journal of differential equations, 1985.

[Golubitsky 2009] Martin Golubitsky, LieJune Shiau, Claire Postlethwaite and Yanyan Zhang. *The Feed-Forward Chain as a Filter-Amplifier Motif*. In Kreimir Josic, Jonathan Rubin, Manuel Matias and Ranulfo Romo, editeurs, Coherent Behavior in Neuronal Networks, numéro 3 de Springer Series in Computational Neuroscience, pages 95–120. Springer New York, January 2009.

[Guckenheimer 1983] J. Guckenheimer and P. J. Holmes. Nonlinear oscillations, dynamical systems and bifurcations of vector fields, volume 42 of *Applied mathematical sciences*. Springer, 1983.

[Haragus 2010] M. Haragus and G. Iooss. Local bifurcations, center manifolds, and

normal forms in infinite dimensional systems. EDP Sci. Springer Verlag UTX series, 2010.

[Hemptinne 2013] Coralie de Hemptinne, Elena S. Ryapolova-Webb, Ellen L. Air, Paul A. Garcia, Kai J. Miller, Jeffrey G. Ojemann, Jill L. Ostrem, Nicholas B. Galifianakis and Philip A. Starr. *Exaggerated phaseamplitude coupling in the primary motor cortex in Parkinson disease*. Proceedings of the National Academy of Sciences, vol. 110, no. 12, pages 4780–4785, March 2013. PMID: 23471992.

[Hoppensteadt 1997] F. Hoppensteadt and E.M. Izhikevich. Weakly connected neural networks. Springer-Verlag New York, Inc., 1997.

[Izhikevich 2007] E.M. Izhikevich. Dynamical Systems in Neuroscience: The Geometry of Excitability And Bursting. MIT Press, 2007.

[Igarashi 2014] Kei M. Igarashi, Li Lu, Laura L. Colgin, May-Britt Moser and Edvard I. Moser. *Coordination of entorhinal-hippocampal ensemble activity during associative learning*. Nature, vol. 510, pages 143-147, June 2014.

[Jadi 2014a] Jadi, M. P., Sejnowski, T. J. *Regulating Cortical Oscillations in an Inhibition-stabilized Network*, Proceedings of the IEEE, 102, 830-842, 2014

[Jadi 2014b] Jadi, M. P., Sejnowski, T. J. *Cortical Oscillations Arise from Contextual Interactions that Regulate Sparse Coding*, Proceedings of the National Academy of Sciences, USA, 111: 6780-6785, 2014

[Jensen 2007] Ole Jensen and Laura L. Colgin. *Cross-frequency coupling between neuronal oscillations*. Trends in cognitive sciences, vol. 11, no. 7, page 267269, 2007.

[Kang 2010] Kukjin Kang, Michael Shelley, James Henrie and Robert Shapley. *LFP spectral peaks in V1 cortex: network resonance and cortico-cortical feedback*. Journal of Computational Neuroscience, vol. 29, no. 3, pages 495–507, 2010.

[Kuznetsov 1998] Yuri A. Kuznetsov. Elements of applied bifurcation theory. Applied Mathematical Sciences. Springer, 2nd édition, 1998.

[Ledoux 2011] Erwan Ledoux and Nicolas Brunel. *Dynamics of Networks of Excitatory and Inhibitory Neurons in Response to Time-Dependent Inputs*. Frontiers in Computational Neuroscience, vol. 5, 2011.

[Lewis 2005] David A. Lewis, Takanori Hashimoto and David W. Volk. *Cortical inhibitory neurons and schizophrenia*. Nature Reviews Neuroscience, vol. 6, no. 4, pages 312–324, April 2005.

[Murphy 2009] B.K. Murphy and K.D. Miller. *Balanced amplification: a new mechanism of selective amplification of neural activity patterns*. Neuron, vol. 61, no. 4, pages 635–648, 2009.

[Neu 1979] John C. Neu. *Coupled Chemical Oscillators*. SIAM Journal on Applied Mathematics, vol. 37, no. 2, pages 307–315, October 1979.

[Newhouse 1978] S. Newhouse, D. Ruelle and F. Takens. *Occurrence of strange AxiomA attractors near quasi periodic flows onT m ,m3*. Communications in Mathematical Physics, vol. 64, no. 1, pages 35–40, December 1978.

[Ostojic 2008] Srdjan Ostojic, Nicolas Brunel and Vincent Hakim. *Synchronization properties of networks of electrically coupled neurons in the presence of noise and heterogeneities*. Journal of Computational Neuroscience, vol. 26, no. 3, pages 369–392, November 2008.

[Ozeki 2009] H. Ozeki, I.M. Finn, E.S. Schaffer, K.D. Miller and D. Ferster. *Inhibitory stabilization of the cortical network underlies visual surround suppression*. Neuron, vol. 62, no. 4, pages 578–592, 2009.

[Paik 2010] Se-Bum Paik and Donald A. Glaser. *Synaptic Plasticity Controls Sensory Responses through Frequency-Dependent Gamma Oscillation Resonance*. PLoS Comput Biol, vol. 6, no. 9, page e1000927, September 2010.

[Pollina 2003] B. Pollina, D. Benardete and V. W. Noonburg. *A Periodically Forced Wilson-Cowan System*. SIAM Journal on Applied Mathematics, vol. 63, no. 5, page 1585, 2003.

[Ray 2011] Supratim Ray and John H. R. Maunsell. *Different Origins of Gamma Rhythm and High-Gamma Activity in Macaque Visual Cortex*. PLoS Biol, vol. 9, no. 4, page e1000610, April 2011.

[Roxin 2005] A. Roxin, N. Brunel and D. Hansel. *Role of Delays in Shaping Spa-*

tiotemporal Dynamics of Neuronal Activity in Large Networks. Physical Review Letters, vol. 94, no. 23, page 238103, 2005.

[Rule 2011] M. Rule, M. Stoffregen and B. Ermentrout. *A Model for the Origin and Properties of Flicker-Induced Geometric Phosphenes*. PLoS computational biology, vol. 7, no. 9, page e1002158, 2011.

[Saleh 2010] K. Saleh and F. Wagener *Semi-global analysis of periodic and quasi-periodic normal-internal k: 1 and k: 2 resonances*. Nonlinearity, vol. 23, 2010

[Schilder 2005] Frank Schilder, Hinke M. Osinga and Werner Vogt. *Continuation of Quasi-periodic Invariant Tori*. SIAM Journal on Applied Dynamical Systems, vol. 4, no. 3, pages 459–488, January 2005.

[Sejnowski 2006] Terrence J. Sejnowski and Ole Paulsen. *Network Oscillations: Emerging Computational Principles*. The Journal of Neuroscience, vol. 26, no. 6, pages 1673 –1676, February 2006.

[Spiegler 2011] Andreas Spiegler, Thomas R. Knsche, Karin Schwab, Jens Haueisen and Fatihcan M. Atay. *Modeling Brain Resonance Phenomena Using a Neural Mass Model*. PLoS Comput Biol, vol. 7, no. 12, page e1002298, December 2011.

[Tsodyks 1997] M.V. Tsodyks, W.E. Skaggs, T.J. Sejnowski and B.L. McNaughton. *Paradoxical effects of external modulation of inhibitory interneurons*. The Journal of neuroscience, vol. 17, no. 11, pages 4382–4388, 1997.

[Vierling-Claassen 2009] Dorea Vierling-Claassen and Nancy Kopell. *The Dynamics of a Periodically Forced Cortical Microcircuit, With an Application to Schizophrenia*. SIAM Journal on Applied Dynamical Systems, vol. 8, no. 2, page 710, 2009.

[Vierling-Claassen 2008] D. Vierling-Claassen, P. Siekmeier, S. Stufflebeam, and N. Kopell *Modeling GABA alterations in schizophrenia: A link between impaired inhibition and altered gamma and beta range auditory entrainment*, J. Neurophysiol., vol 99, pp. 2656-2671, 2008

[Wedgwood 2013] Kyle CA Wedgwood, Kevin K Lin, Ruediger Thul and Stephen Coombes. *Phase-Amplitude Descriptions of Neural Oscillator Models*. The Journal of Mathematical Neuroscience, vol. 3, no. 1, page 2, 2013.

[Wilson 1972] H.R. Wilson and J.D. Cowan. *Excitatory and inhibitory interactions in localized populations of model neurons*. Biophys. J., vol. 12, pages 1–24, 1972.

[Womelsdorf 2012] T. Womelsdorf, B. Lima, M. Vinck, R. Oostenveld, W. Singer, S. Neuenschwander and P. Fries. *Orientation selectivity and noise correlation in awake monkey area V1 are modulated by the gamma cycle*. Proceedings of the National Academy of Sciences, February 2012.

[Wright 2012] Wright Barry, Alderson-Day Ben, Prendergast Garreth, Bennett Sophie, Jordan Jo, Whitton Clare, Gouws Andre, Jones Nick, Attur Ram, Tomlinson Heathera and Green Gary *Gamma Activation in Young Peo-*

ple with Autism Spectrum Disorders and Typically-Developing Controls When Viewing Emotions on Faces, PLoS ONE, Volume 7, Issue 7, 2012

[Zhang 2011] Yanyan Zhang and Martin Golubitsky. *Periodically Forced Hopf Bifurcation*. SIAM Journal on Applied Dynamical Systems, vol. 10, no. 4, page 1272, 2011.